Surface-Enhanced Raman Scattering Hybrid Nanoprobe Multiplexing and Imaging in Biological Systems

Andrea Matschulat,[†,‡] Daniela Drescher,[†,‡] and Janina Kneipp[†,‡,*]

[†]Federal Institute for Materials Research and Testing, Richard-Willstätter-Strasse 11, 12489 Berlin, Germany, and [‡]Humboldt-Universität zu Berlin, Department of Chemistry, Brook-Taylor-Strasse 2, 12489 Berlin, Germany

ABSTRACT Surface-enhanced Raman scattering (SERS) labels and probes consisting of gold and silver nanoaggregates and attached reporter molecules can be identified by the Raman signature of the reporter molecule. At the same time, SERS hybrid probes deliver sensitive molecular structural information on their nanoenvironment. Here we demonstrate full exploitation of the multifunctional and multiplexing capabilities inherent to such nanoprobes by applying cluster methods and principal components approaches for discrimination beyond the visual inspection of individual spectra that has been practiced so far. The reported results indicate that fast, multivariate evaluation of whole sets of multiple probes is feasible. Spectra of five different reporters were shown to be separable by hierarchical clustering and by principal components analysis (PCA). In a duplex imaging approach in live cells, hierarchical cluster analysis, *K*-means clustering, and PCA were used for imaging the positions of different types of SERS probes along with the spectral information from cellular constituents. Parallel to cellular imaging experiments, cytotoxicity of the SERS hybrid probes containing aromatic thiols as reporters is assessed. The reported results suggest multiplexing applications of the nontoxic SERS nanoprobes in high density sensing and imaging in complex biological structures.

KEYWORDS: surface-enhanced Raman scattering · nanosensor · *para*-aminobenzenethiol · 2-naphthalenethiol · 3T3 cells · principal component analysis · hierarchical cluster analysis · cytotoxicity · imaging

The increase in Raman scattering signals from molecules in close proximity to a noble metal nanostructure,[1−6] known as surface-enhanced Raman scattering (SERS), has been made use of in a number of bioanalytical applications, ranging from immunoassays to intracellular studies. Apart from sensitive detection of analytes, SERS enables the construction of optical labels using enhanced Raman signals as a spectroscopic signature.[7−10]

SERS labels are hybrids consisting of metal nanostructures, typically combinations of aggregates of gold or silver nanoparticles and reporter molecules. SERS labels can be functionalized with specific antibodies, peptides, and DNA in order to achieve specific recognition or targeting.

With respect to their reporting capabilities, there are two types of SERS labels: In a first type, unprotected monolayers of reporter molecules on metal nanoparticles are used,[11−13] or the SERS label (metal nanoparticle plus reporter) is covered by a protective layer of glass or polyethylene glycol.[14−17] The advantages of these coated and uncoated SERS labels or tags include physical robustness, stable signals, and immunity to their biological and chemical environment. Overall, despite these essential technical advantages, this type of SERS label exhibits the same function as a fluorescence tag, that is, highlighting and imaging a biological structure based on the optical signature of the reporter.

The second type does not use such a protective cover; we call them in the following SERS hybrid probes.[18,19] The main advantage of these SERS hybrid probes lies in their multifunctionality: SERS hybrid probes can be identified by the signature of a reporter molecule. Based on the surface-enhanced Raman signal generated also by other molecules present in the local optical fields of the metal nanoaggregates, at the same time, they deliver sensitive molecular structural information on their (biological) nanoenvironment. Therefore, hybrid probes are different from typical SERS tags, as the latter do not provide information from other molecules except the reporter.[7,15,20]

Regarding label composition, in many cases, reporter molecules are in fact fluorescent dyes. The advantages of SERS labels compared to common labels used in fluorescence can be found in an enormous multiplexing potential due to the fingerprint-like nature of the vibrational spectrum. Moreover, in SERS, excitation can be out-of-resonance with electronic transitions of a reporter molecule. This prevents photodegeneration and results in a high stability of SERS labels. Additionally, it provides the free

*Address correspondence to janina.kneipp@chemie.hu-berlin.de.

Received for review February 10, 2010 and accepted May 11, 2010.

Published online May 26, 2010. 10.1021/nn100280z

TABLE 1. Characteristic Band Ratios in the SERS Spectra of Six Reporter Molecules Obtained with Silver Nanoparticles That Were Used for the Chemical Identification of Each Reporter

	*p*ABT	RBITC	2-NAT	CV	*p*MBA	FITC
band positions (cm^{-1})	1078/390	1357/1075	1068/1624	1175/1620	363/527	1182/372
ratio	0.5 ± 0.2	3.4 ± 0.5	3.9 ± 0.6	3.1 ± 0.4	3.2 ± 0.3	1.1 ± 0.2
number of spectra	99	38	40	51	25	19

choice of excitation wavelength (and therefore, also detection range) as yet another significant advantage over fluorescence labels. Additional gain in sensitivity for a SERS label can result when excitation occurs in resonance with electronic transitions in the reporter molecules, so that an additional resonance enhancement, termed surface-enhanced resonant Raman scattering (SERRS) is employed.[11,21] The high sensitivity of SERRS labels is paid for with a limited range of excitation wavelengths in label detection.

Experiments relying on the detection of the SERS spectral signature of the reporter include the introduction of SERS probes into organisms and attachment to the surface of cells as targeting agents of specific surface markers.[15,17,22] Inside the cellular interior, spectra of specific individual Raman labels have been imaged.[23−25]

In several cellular processes, simultaneous investigation of different locations is favorable. To achieve this, a specific SERS hybrid probe must identify itself as being of a specific type, for example, with respect to its targeting. Therefore, it is useful to introduce with each probe type a probe-specific signature that allows identification. In such a multiplexing approach with different types of SERS hybrid probes, each probe also enables investigation of its specific cellular environment.

In previous work, we and others have generated SERS hybrid probes for intracellular studies.[18,19] Although the multiplexing potential of both conventional SERS tags and hybrid SERS probes has been pointed out, all studies have so far used the mere visual inspection of reporter spectra or intensity mapping of one band for analysis.[7,8,18,20,26] Fast methods or multivariate statistics were not applied, despite the fact that the greatest potential of SERS labels and probes surely lies in the efficiency provided by multivariate methods for their fingerprint-based imaging. Automated identification will be crucial particularly for intracellular or sensing applications.

Here we demonstrate the full exploitation of the multiplexing capabilities inherent to SERS nanoprobes and labels by the application of fast, multivariate methods. We study the SERS spectra of five reporter molecules by multivariate methods. We have based identification of the reporter spectra on both, two specific spectral positions and the intensity ratio of these bands. Hierarchical clustering and principal components analysis were used for separation of different reporter spectra both on silver and on gold nanoparticles. In a second step, we apply simultaneously different SERS hybrid probes in multivariate imaging experiments with cultured cells. Parallel to the experiments in a duplex SERS imaging approach, cytotoxicity of the SERS hybrid probes is assessed.

RESULTS AND DISCUSSION

Chemical Separation of SERS Reporter Signatures. SERS spectra of six different Raman reporter molecules measured on silver and gold nanoaggregates are displayed in Figure 1. Five of them, *para*-aminobenzenethiol (*p*ABT), rhodamine (B) isothiocyanate (RBITC), crystal violet (CV), 2-naphthalenethiol (2-NAT), and *p*-mercaptobenzoic acid (*p*MBA) provide strong, typical vibrational signatures with both silver and gold nanoparticles. In addition, the characteristic SERS spectra of fluorescein isothiocyanate (FITC) and of 5,5′-dithiobis(2-nitrobenzoic acid) (DTNB) can be used as reporter signatures on silver and gold nanoparticles, respectively (compare last spectra in Figure 1 panels A and B, respectively). For a discussion of the spectral features of all these potential reporter molecules, also in the context of concentration and possible interaction with different types of SERS substrates, the reader is referred to previous basic studies, e.g., to refs 27−32. Labels and probes containing one of these molecules at a time as reporter have also been applied in cells, as was the case for CV,[18,25] 2-NAT,[33] and *p*MBA.[23,34] In these spatially resolved one-reporter experiments, the position of the particular reporter was imaged by so-called chemical mapping, that is, based on the intensity of one band or one intensity ratio that was selected from the SERS spectrum.

"Chemical" parameters in the spectrum of each of the six reporters used in our study here can also be used for their discrimination in a multiplex experiment.

TABLE 2. Characteristic Band Ratios in the SERS Spectra of Six Reporter Molecules Obtained with Gold Nanoparticles That Were Used for the Chemical Identification of Each Reporter

	*p*ABT	RBITC	2-NAT	CV	*p*MBA	DTNB
band positions (cm^{-1})	1081/390	1357/1183	1380/368	1172/1584	1078/524	1338/1555
ratio	1.3 ± 0.5	1.5 ± 0.5	1.7 ± 0.1	6.3 ± 0.4	2.0 ± 0.2	10 ± 2
number of spectra	31	48	99	51	34	26

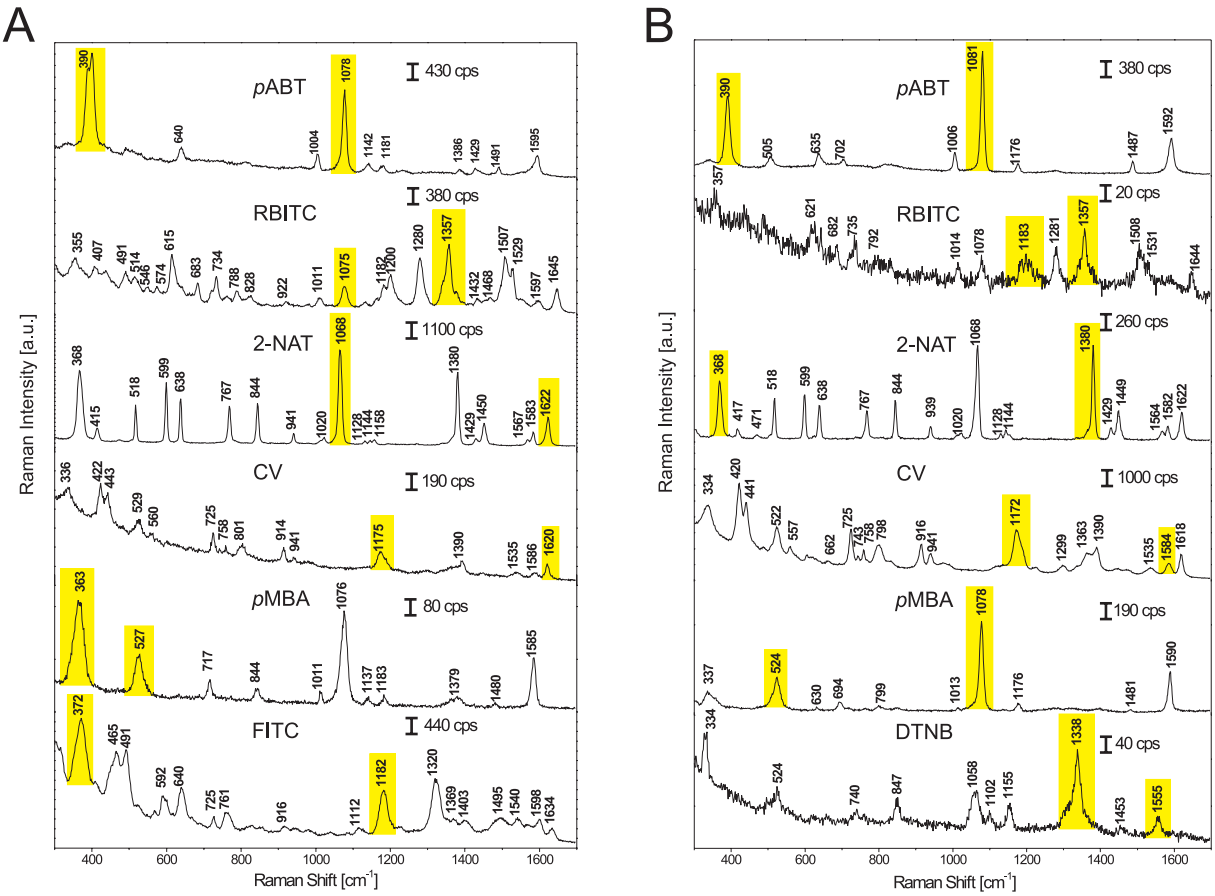

Figure 1. Example SERS spectra of the five reporters *p*ABT, RBITC, 2-NAT, CV, and *p*MBA (A) on silver and (B) on gold nanoaggregates. The sixth spectrum in panel A and B is of the fluorescent dye FITC and of DTNB, respectively. Excitation wavelength: 785 nm, excitation intensity ~8 × 10^4 W/cm^2, accumulation time: 1 s. Abbreviations: *p*ABT, *para*-aminobenzenethiol, RBITC, rhodamine (B) isothiocyanate, CV, crystal violet, *p*MBA, *p*-mercaptobenzoic acid. The bands used for chemical analysis of the spectra (compare Tables 1 and 2) are highlighted in yellow.

Two data sets were generated, containing 272 and 289 SERS spectra of six different reporter molecules on silver and gold nanoaggregates, respectively. As shown in Tables 1 and 2, one particular ratio of two bands can be used to identify the characteristic spectrum of each reporter molecule in a mixed set of reporter spectra. As the spectral intensity in a SERS experiment may fluctuate considerably, utilization of a band ratio ensures the stability of the identification parameter. The bands that were used for calculation of the intensity ratio are highlighted in each of the example spectra in Figure 1.

In a common chemical imaging or identification approach, one intensity, intensity ratio, or band position is determined for each spectrum. In a SERS experiment, slight shifts in the position of Raman bands due to the different local environment of the molecules can occur. Therefore, separation based on one individual parameter, such as intensity ratio or band position can hamper distinction between different reporter spectra. Here, we have based identification of the reporter spectra on both, two specific spectral positions and the intensity ratio of these bands. Discrimination of the very similar spectra of *p*ABT and *p*MBA (compare Figure 1) by this trivariate approach illustrates its robustness. In analytical applications with known reporters and their specific intensity ratios, for example, SERS tags in array format hybridization or immunoassays, the automated comparison of intensity ratios of selected marker bands could easily be applied for fast identification.

Multivariate Discrimination of Five SERS Reporter Signatures. To achieve identification and separation of reporter molecules in unknown mixtures or in the presence of additional analyte molecules, for example, in the case of SERS hybrid probes in a biological environment, multivariate methods that consider the whole spectral fingerprint are clearly of advantage. Principal components analysis (PCA) is a useful statistical technique that has found application in fields such as pattern recognition[35] and image compression,[36] and has become a common technique for finding patterns in data of high dimension, in particular in hyperspectral mapping and characterization approaches.[37−39] The spectral differences in the data sets comprising 263 spectra of the reporter molecules *p*ABT, RBITC, CV, 2-NAT, and *p*MBA on gold nanoparticles were analyzed by PCA. Briefly, the data matrix, consisting of 263 spectra with 961 data points (covering the spectral range 300−1700 cm^{-1}) was projected into a new, variance-weighted coordinate sys-

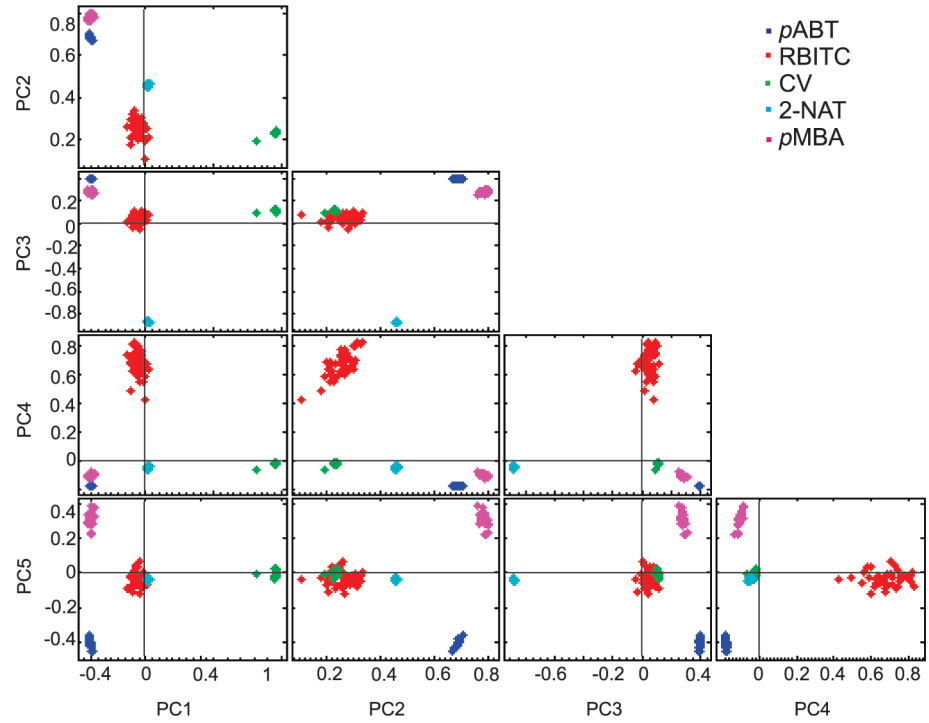

Figure 2. Plots of the first five principal components scores obtained in PCA with 263 spectra of the five reporter molecules *p*ABT, RBITC, CV, 2-NAT, and *p*MBA on gold nanoparticles. PCA was performed with vector-normalized first derivative spectra over the spectral range 300−1700 cm^{-1}.

tem. This mathematical procedure (orthogonal linear transformation or eigenvalue problem) transforms a number of possibly correlated variables of the spectral data set into a smaller number of uncorrelated variables such that the greatest variance by any projection of the data comes to lie on the first coordinate.[40] Figure 2 shows the scores plots of the first five principal components (PCs) against one another. These plots illustrate that the five different reporter signatures can be separated readily using three of the first four PCs. For example, *p*ABT, 2-NAT, and *p*MBA separate well along PC2 and PC3 and CV and RBITC separate well along PC4 (compare plot of PC2 vs PC4 in Figure 2).

Hierarchical cluster analysis (HCA) utilizing the information over the same spectral range from 300−1700 cm^{-1} also provides evidence that the whole spectral fingerprint can be used for discrimination of the five different reporter signatures in the test data sets (Figure 3). The resulting dendrograms were obtained in cluster analyses with vector-normalized first-derivative spectra. They contain five separate classes and illustrate that variance within the group of spectra of each reporter is much smaller than interclass variance. At this point it should be noted that signal-to-noise ratio varied not only between different SERS labels but in particular within each group of particular reporter. The dendro-

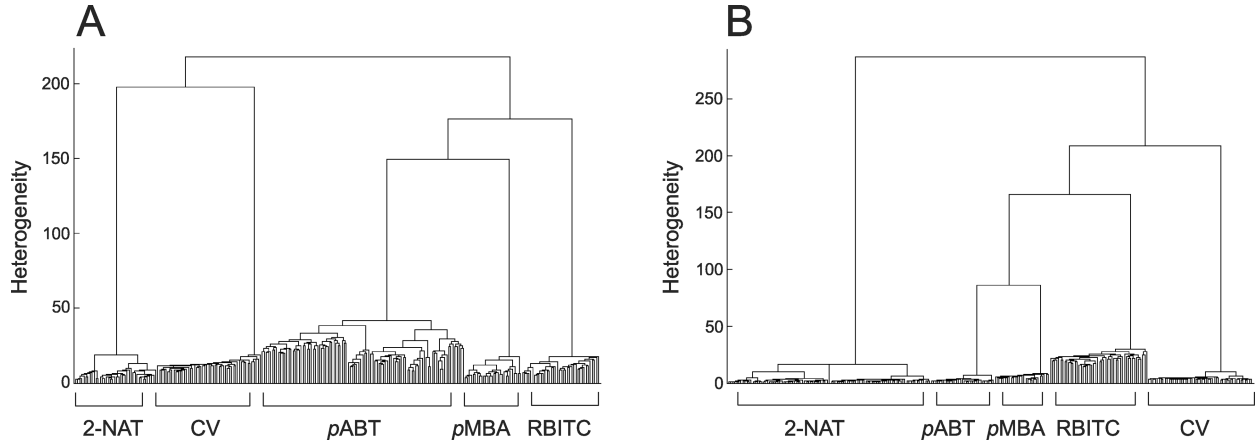

Figure 3. Results of hierarchical cluster analysis of (A) 253 reporter spectra of the five reporter molecules *p*ABT, RBITC, CV, 2-NAT, and *p*MBA obtained with silver and (B) 263 spectra obtained with gold nanoparticles. HCA was performed with vector-normalized first-derivative spectra in the spectral region 300−1700 cm^{-1} using Ward's algorithm and Euclidean distance measure.

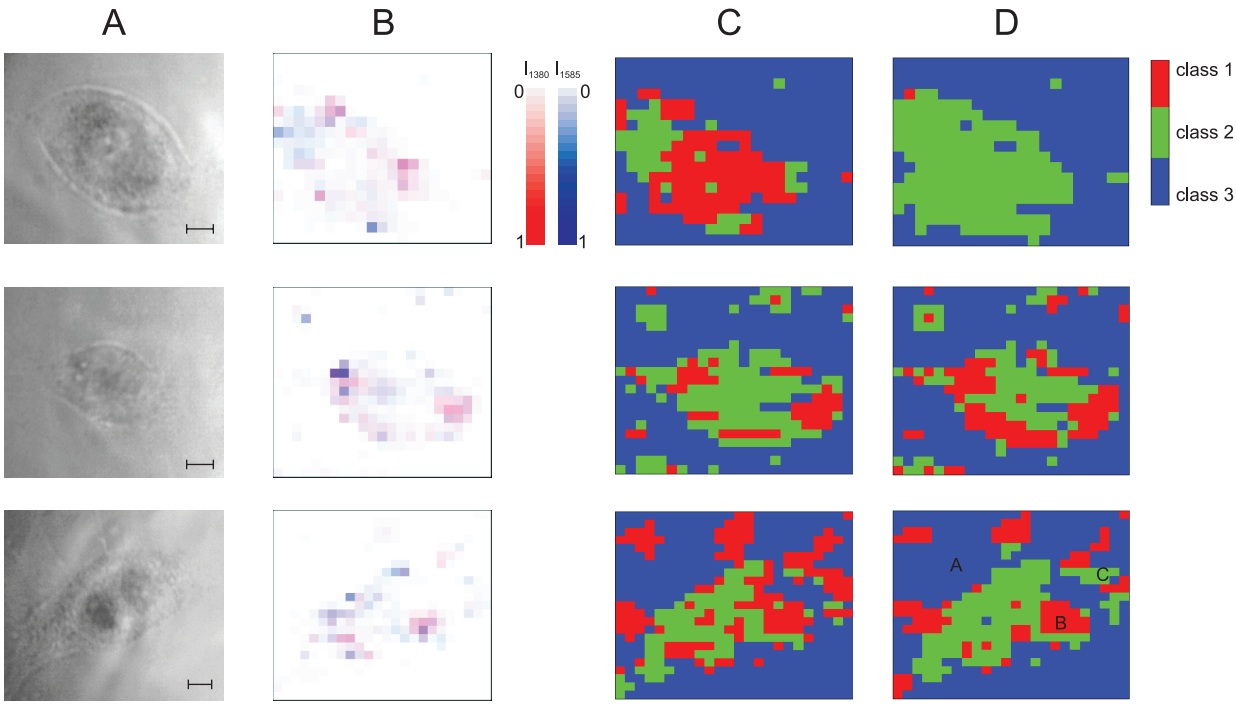

Figure 4. (A) Photomicrographs, (B) chemical images, (C) HCA, and (D) *K*-means cluster maps of three 3T3 cells (map sizes, from top to bottom: 21 × 18 spectra, 23 × 21 spectra, and 24 × 23 spectra). Scale bar of panel A = 4 μm. The image in panel B was generated by superposition of two images, based on the intensity of the C−C stretching of *p*ABT at ~1585 cm^{-1} (blue scale) and a 1380 cm^{-1} ring stretching mode of 2-NAT (red scale). All band intensities were normalized between the lowest color value (0) and highest color value (1). Multivariate cluster maps (C and D) were based on three classes and spectral information in the region 300−1700 cm^{-1}, of vector-normalized first derivative spectra. HCA used Euclidean distance and Ward's algorithm. The labels in the last image of panel D indicate position of example spectra in Figure 5.

grams also reflect a high level of similarity of the spectra of *p*ABT and *p*MBA with one another, compared to the spectra of the other molecules. HCA can help to find SERS signatures of high dissimilarity. This can be important especially when more than one reporter is used in addition to existing spectral contributions, for example, from an analyte, as in the case of SERS hybrid probes for intracellular applications.

Duplex Imaging in Living Cells Using *p*ABT and 2-NAT SERS Hybrid Probes. As an application of SERS probes with different reporter molecules, we incorporated two types of SERS hybrid probes consisting of *p*ABT and 2-NAT, respectively, on gold nanoaggregates into the endosomal system of 3T3 fibroblast cells. Exposure to *p*ABT probes for 30 min was followed by 1 h delay, then, the probes containing 2-NAT as reporter were administered. All excess probes were removed by thorough washing. An intracellular aggregation of incorporated gold nanoparticles was not clear from light microscopy owing to the relatively short incubation time of 30 min (Figure 4A). However, uptake of the hybrid probes could be confirmed by the appearance of surface-enhanced Raman signals collected from the cellular interior.

Figure 4B shows chemical maps of 3T3 cells simultaneously containing the two different probes. Each pixel in the map represents one Raman spectrum. Band intensities specific for the two reporters (C−C stretching vibration of *p*ABT ≈ 1585 cm^{-1} and ring stretching vibration of 2-NAT ≈ 1380 cm^{-1}) were normalized between the highest and lowest value (scaled from white to blue for *p*ABT, white to red for 2-NAT) and superimposed. As a result, purple pixels represent mixed spectra containing information of both reporter molecules. In addition, cellular regions were found that contained mainly *p*ABT probes (blue pixels in Figure 4B).

For spectral mapping, we applied HCA as an unsupervised method, supervised *K*-means cluster analysis, as well as PCA. HCA-based maps for the three example cells are displayed in Figure 4C, the *K*-means maps are shown in Figure 4D. In the cluster maps, each spectrum, that is, each pixel is assigned a color, corresponding to its classification. Both analyses suggest that the spectra can be grouped into three major classes.

Although both cluster methods differ significantly, the three clusters obtained with both of them seem to be composed of roughly the same spectra (compare Figures 4 panels C and D). This may be because both methods use a quite similar cluster goal criterion.[41] This cluster criterion describes the process of arrangement of objects leading to maximization of the variance between two clusters, whereas intracluster variance is minimized. However, assignments of spectra to the three classes are not fully identical for HCA and *K*-means analysis. This is because during the process of cluster fusion in HCA, objects are classified stepwise according to their smallest distance, leading to bigger clusters. In

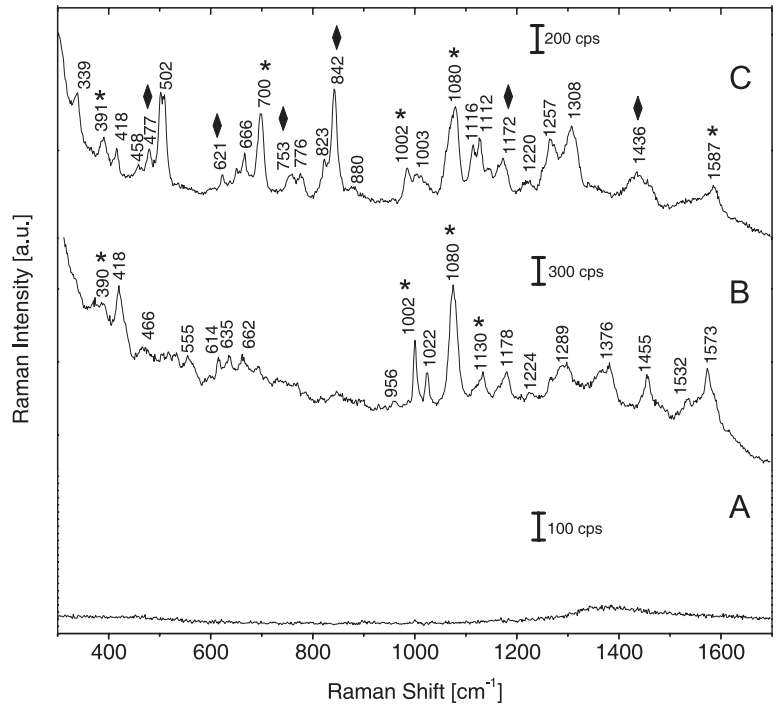

Figure 5. Characteristic SERS spectra for each of the three classes identified in *K*-means cluster analysis (*cf.* labels in Figure 4D last row): (A) spectrum without SERS signals, obtained at a position where no nanoprobes were present; (B) spectrum containing SERS signals of *p*ABT (*) and cellular molecules; (C) spectrum with SERS signatures of both reporters, *p*ABT (*), and 2-NAT (♦).

the next step, objects with smaller distances are combined. During this irreversible process, a hierarchical grouping is generated.[41] *K*-means incidentally assigns *n* objects to *K* clusters calculating the Euclidean distances between these objects and cluster-centers (centroids). Therefore, in contrast to hierarchical methods, the assignments of objects to certain clusters may change during recalculations of the cluster centers.

Figure 5 shows an example spectrum for each of the three clusters (compare third *K*-means map in Figure 4D). Obviously, one class contains all spectra without SERS signals (Figure 5, spectrum A). The other two clusters consist of spectra with SERS signals. According to the multifunctionality of the SERS probes,[18] all spectra contain contributions from molecules of the cell, that is, from the endosomal environment of the probes. As control, spectra were also acquired with the probes in cell culture medium, indicating no contribution from molecules of the culture medium the probes were administered with (Supporting Information). Possible assignments of the cellular contribution were provided in earlier papers.[42] One of the clusters comprises all spectra that display characteristic bands of *p*ABT alongside those of molecules from the cell (*cf.* spectrum B). The other group of spectra shows bands of 2-NAT together with those of *p*ABT, and less contributions from cellular molecules.

Since the different reporter contributions in the spectra of class 2 (*cf.* Figure 4D and 5) come from different probe types, one sampled spot must contain more than one probe. Regarding localization of the two types of hybrid probes with respect to cellular ultrastructure, this type of mixed reporter spectrum can in principle be generated from two situations: (i) the fL-probed volume contains different vesicles, each surrounding a different type of hybrid probe and (ii) larger endosomal structures, generated by endosomal fusion processes,[43,44] that contain several hybrid probes of both probe types. We have observed such structures before in experiments with bare SERS nanoprobes and parallel TEM studies.[42] Which of the situations is the case in the duplex experiment here cannot be resolved with the current data, but different targeting of different probe types in future applications will clarify this situation. Cluster imaging is based on all signals of the hybrid probes, including those of cellular molecules in the probes' proximity, and takes into account also varying relative intensities in different spectra of the same reporter molecule caused, for example, by varying orientation or concentration effects. Thereby, better contrast can be generated than in chemical images. For example, in Figure 4 panels C and D, the filamentous branches as characteristic morphological features of fibroblast cells become evident.

The first derivatives of all mapping data were also subjected to PCA. To use overall variance for generation of image contrast, an image was generated based on the scores of each PC. Examples of such PC images are displayed in Figure 6 for one selected data set (same data set as last row of Figure 4). Comparison with the cluster image results (last row of Figure 4D) reveals that PC1, which points into the direction of greatest vari-

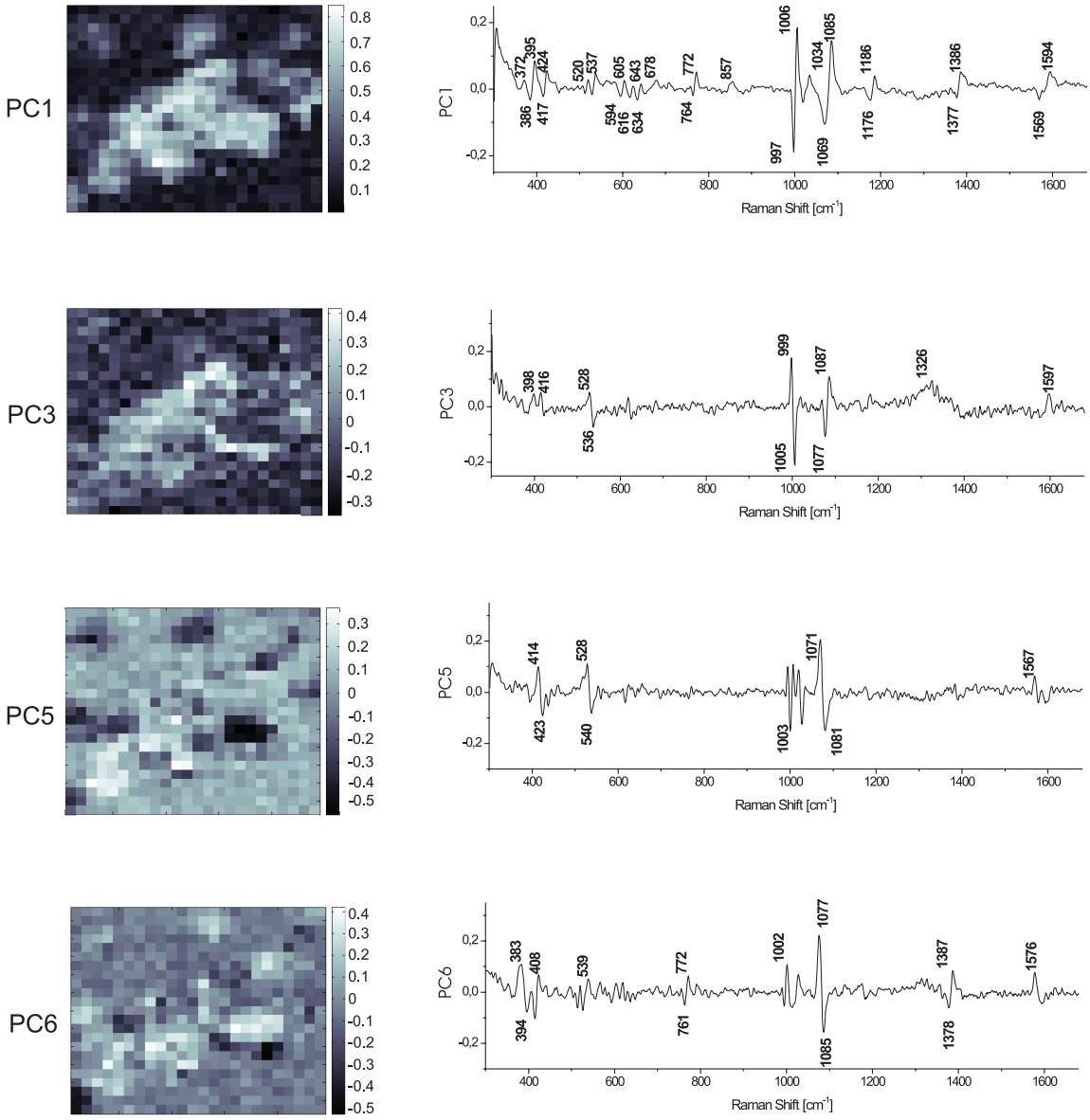

Figure 6. PCA score maps of a 3T3 cell in SERS experiment with *p*ABT and 2-NAT hybrid probes (left) and corresponding loadings spectra (right) for four PCs. The mapping data set consisted of 552 spectra (same data set as in last row of Figure 4).

ance in the data set, can be used to image all spectra with SERS signal (bright pixels in the first panel of Figure 6). Accordingly, the loading spectrum of PC1 contains features at all frequencies where characteristic bands of the reporter molecules *p*ABT and 2-NAT, as well as characteristic bands of cellular molecules, are located. Using PC3, contrast can be generated between spectra containing contributions from both reporter molecules as opposed to the other spectra in the data set. Note that the locations of high scores for PC3 correspond well with the distribution of class C spectra in the *K*-means cluster map (compare PC3 image of Figure 6 with Figure 4D last row). The same is the case for PC5. In contrast, the image of PC6 indicates differences in 2-NAT spectral contributions. High PC6 scores colocalize with class B spectra in the *K*-means cluster map (compare PC6 image of Figure 6 with Figure 4D last row), those with mainly *p*ABT bands, but scarce 2-NAT signals. It should be noted that in the case of the intense band at ~1002 cm^{-1}, there occurs superposition of a characteristic band of *p*ABT with the ring breathing mode of the cellular molecule phenylalanine (*cf., e.g.*, Figure 5, spectrum B). Variance in the presence of phenylalanine is found in almost every PC. Similar results were found for all other data sets that have been analyzed in these experiments.

Impact of Reporter Molecules and SERS Hybrid Probes on Cellular Viability. To obtain meaningful data using SERS hybrid probes in live cells, more than fast data analysis methods have to be implemented. In particular in the

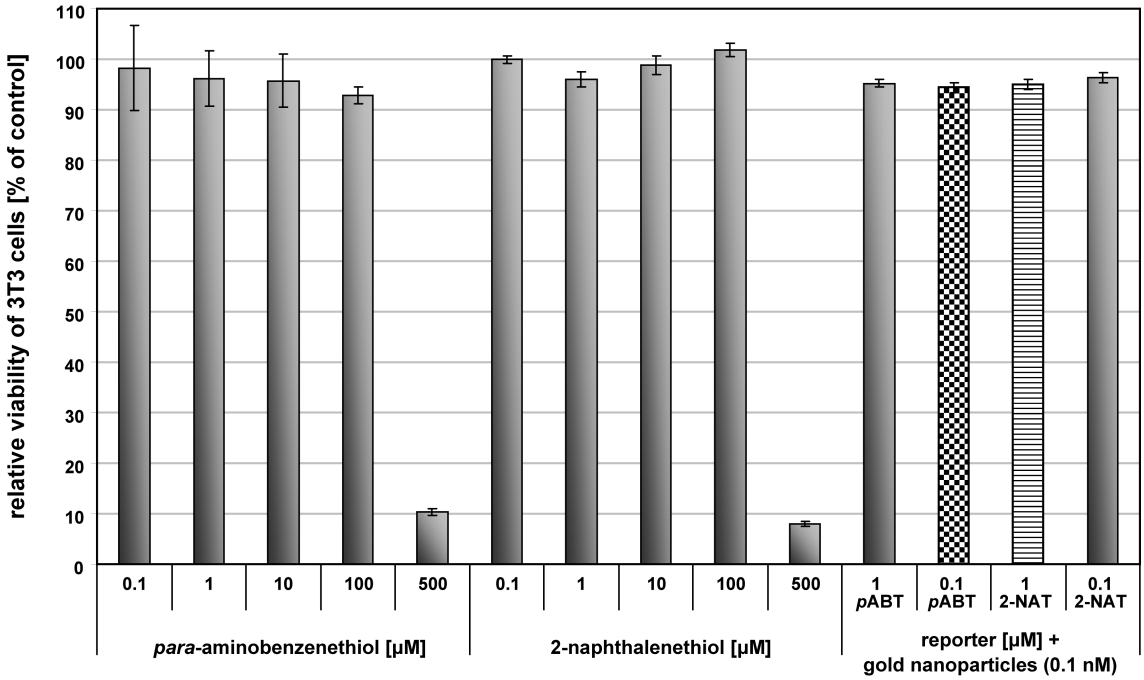

Figure 7. Viability of 3T3 cells after 24 h-exposure to different concentrations of *para*-aminobenzenethiol (*p*ABT) and 2-naphthalenethiol (2-NAT) in culture medium as determined by XTT assay (mean value ± margin of deviation of four replicates). The cytotoxic effect of the gold nanoprobes with the corresponding reporter on 3T3 cells, as used in SERS experiments, was also assigned (bars are highlighted).

context of large reporter libraries, the influence of the probes on the status of the biological system has to be studied. Toxicity of gold[45−52] and silver nanoparticles[53−56] has been extensively investigated. All nanoprobes used in our study were internalized by endocytosis from the cell culture medium over a time of 30 min.

The major issue, that has, however, only been rarely addressed so far is the toxicity of probes containing the reporter molecules, and of the reporter molecules themselves. So far, in many cases, biocompatible dyes, such as indocyanine green or Rose Bengal have been applied and assumed to be nontoxic.[18,19] However, creating great arsenals of different reporters for live cell multiplex approaches will require an assessment of their potential cytotoxicity.

The toxicity of aromatic thiols (benzenethiol and *para*-aminobenzenethiol) in blood cells was shown in early work.[57] For example, oxidative stress can be induced in the cells using *p*ABT at a concentration of 0.25 mM in cell culture medium.

Although the concentration of the reporter molecules in our experiments was much lower (maximum of 10^{-7} M for *p*ABT and 10^{-6} M for 2-NAT), we investigated cell viability for the conditions used in our SERS imaging experiments using a standard XTT assay. This assay enables conclusions on viability based on the activity of intramitochondrial dehydrogenase of the cells.[58]

The results of this assay, conducted for five concentrations of each reporter *p*ABT and 2-NAT, and both reporters on gold nanoparticles at possible conditions for a SERS imaging experiment are displayed in Figure 7. After an incubation of 24 h with both *p*ABT and 2-NAT in concentrations $\leq 10^{-4}$ M, the cells display >90% viability. However, reporter concentrations $>10^{-4}$ M have a significant influence on metabolic activity of the cells (Figure 7). Control experiments also showed that the small content in methanol used for dissolving *p*ABT does not have an influence on cytotoxicity. The same 24 h incubation and subsequent XTT assay was also conducted for SERS hybrid probes containing *p*ABT and 2-NAT in two concentrations on gold nanoparticles (10^{-10} M particle concentration). After 24 h incubation with such probes, viability of the cells was observed to be 95% of that of control cells. This is in good agreement with results for plain gold nanoparticles.[45,46,48]

CONCLUSIONS

Spectra of different reporters were shown to be separable by hierarchical clustering and by PCA. In a duplex imaging approach in live cells, hierarchical cluster analysis, *K*-means clustering, and PCA were used for imaging the positions of two different types of SERS probes along with the spectral information from cellular constituents. The results of cluster methods and principal components approaches for discrimination indicate the potential capabilities of SERS nanoprobes.

From the cytotoxicity experiments we can conclude that neither free reporter molecules nor SERS hybrid probes are toxic to standard cultured cells at concentrations used in typical SERS experiments, even if incuba-

tion times are of a much longer duration than in the experiments conducted here. The biocompatibility of SERS hybrid probes, along with the imaging capabilities provided by the multivariate analyses suggests fast SERS multiplexing in complex systems. In particular, the examples used in our experiments suggest that various aromatic thiols could form a basis for a large set of different SERS hybrid nanoprobes for sensitive live cell probing.

The results of cluster methods and principal components approaches for discrimination indicate that fast, multivariate evaluation of whole sets of multiple probes is feasible, beyond the visual inspection of individual spectra that has been practiced so far, and also for varying signal-to-noise ratio. This suggests multiplexing applications with SERS hybrid nanoprobes and SERS tags in very high density sensing and biological imaging applications, where fast read-out is required.

METHODS

Chemicals and Materials. For preparation of colloidal solutions of gold and silver nanoparticles in water, silver nitrate (99.9999%, Sigma-Aldrich), gold(III) chloride trihydrate (99.9%, Sigma-Aldrich), and trisodium citrate dihydrate (99%, Merck) were purchased. Different reporter molecules such as *p*-mercaptobenzoic acid (95%, Chempur), 2-naphthalenethiol (>99%, Fluka), *para*-aminobenzenethiol (97%, Aldrich), crystal violet (>90%, J.T.Baker), fluorescein isothiocyanate (90%, Sigma), rhodamine (B) isothiocyanate (>70%, Sigma), 5,5′dithiobis(2-nitrobenzoic acid) (98%, Sigma) as well as sodium chloride (99.99%, Merck) for electrolyte solutions and methanol (99.8%, J.T.Baker) as solvent were purchased. For all experimental procedures, ultrapure water (18 MΩ) was applied.

For SERS experiments, silver nanoparticles were synthesized according to a modified protocol of Lee and Meisel which was also described by Aroca[6] and Munro *et al*.[59] Gold nanoparticles were synthesized according to a modified protocol of Lee and Meisel.[60] In electron microscopy, a size distribution of the gold nanoparticles was determined to range from 20 to 50 nm, and for colloidal silver from 20 to 60 nm. The extinction spectra of silver and gold nanoparticle solutions show characteristic positions of the plasmon resonance band of the colloidal silver and gold to be at 440 and 532 nm, respectively. In our studies, silver and gold nanoparticles gave rise to a similar strong SERS enhancement (EF ≈ 10^6).

Stock solutions of the reporter molecules *para*-aminobenzenethiol (*p*ABT), 2-naphthalenethiol (2-NAT), rhodamine (B) isothiocyanate (RBITC), fluorescein isothiocyanate (FITC), and crystal violet (CV) were prepared in methanolic solutions, whereas *para*-mercaptobenzoic acid (*p*MBA) and 5,5′-dithiobis(2-nitrobenzoic acid) (DTNB) stock solutions were prepared in 0.01 M phosphate-buffered saline solution (PBS, pH ≈ 7.3) and 0.1 M phosphate-buffered solution (PB, pH ≈ 7.3) respectively. Further dilutions of reporter-containing methanolic solutions were then performed in 0.01 M PBS buffer to provide a biocompatible environment.

Delivery of SERS Hybrid Probes to Cells. Mouse fibroblast cells (3T3; DSMZ, Braunschweig, Germany) were grown on sterile coverslips (Thermo Fisher Scientific, Waltham, U.S.A.) in 6-well culture plates for 24 h in Dulbecco's modified eagle medium (referred to as DMEM; Biochrom AG, Berlin, Germany) supplemented with 10% fetal calf serum, 100 units/mL penicillin and 100 μg/mL streptomycin (Biochrom AG) at a density of ~10^4 cells/cm^2 in a controlled environment (37 °C, 5% CO_2).

Prior to the experiment, the gold nanoparticle suspension (final particle concentration: 10^{-10} M) was mixed with the reporter solution (final concentration: *p*ABT 10^{-7} M; 2-NAT 10^{-6} M), diluted with cell culture medium and immediately applied to the cells. The hybrid nanoprobes were delivered to 3T3 cells in two separate steps by fluid phase uptake. First, the standard medium was replaced by culture medium including *p*ABT hybrid probes at a concentration of 10^{-7} M. After an exposure time of 30 min, the cells were washed with PBS buffer solution (Biochrom AG) and continued to grow in pure culture medium for 1 h. In the second step, 2-NAT nanoprobes at a concentration of 10^{-6} M in the culture medium were used for incubation for 30 min. The 2-NAT gold pulse was followed by 1 h of incubation in standard culture medium without any nanoprobes. Thereby, endosomes containing *p*ATP probes were of a different age than those containing 2-NAT probes. Upon completion of the incubation steps, the cells were washed thoroughly with PBS buffer and immediately transferred to the Raman microscope, where the SERS spectra were obtained from live cells in PBS buffer.

Raman Experiments. All Raman experiments were performed with a Raman microspectroscopic setup (LabRam, Horiba-Jobin-Yvon, Bensheim, Germany). SERS spectra were measured using a 60× microscope water immersion objective. A spectrograph with notch filter in the front of the entrance slit and a liquid nitrogen-cooled CCD detector were used for spectral dispersion and collection of the scattered light. An excitation wavelength of 785 nm, that is, out-of-resonance with transitions in the reporter molecules, was applied in all measurements.

The concentration of reporter molecules in the Raman experiments on gold and silver nanoparticles outside cells was 10^{-5} M, except for *p*MBA with 10^{-7} M. In UV/vis control experiments no aggregation was observed upon addition of the reporter molecules to the silver nanoparticles, except for CV. Absorption spectra of the gold nanoparticles revealed the formation of small aggregates. All substrates remained stable even at time intervals that were much longer than the time frame of the Raman experiments.

For studies of eukaryotic cells, measurements were carried out as raster scans in 2 μm steps over single living 3T3 cells with a computer-controlled *xy*-stage. The laser spot size formed through the objective led to a spot size of ~1.8 μm. Excitation intensity in all experiments was approximately 8 × 10^4 W/cm^2. Acquisition time for all spectra was 1 s.

Data analysis. Cosmic spike removal was done with CytoSpec 1.4 hyperspectral imaging software.[61] CytoSpec 1.4 was also used to calculate ratios of the integrated areas of two bands ("chemical" analysis).

Data analysis of the reporter spectra on gold and silver was carried out on two data sets containing 289 and 272 spectra, respectively, of six different reporters. Spectra of five of the reporters, *p*ABT, 2-NAT, RBITC, CV, and *p*MBA were obtained both on gold and on silver nanoparticles. To be able to compare the outcome of the multivariate analyses on the two types of nanoparticles, the spectra of the sixth reporter species, FITC on silver nanoparticles and NTB^{2-} (residue of DTNB) on gold nanoparticles, were not included in the hierarchical cluster analysis and principal components analysis. This yielded two data sets of 256 spectra for silver nanoparticles and 263 spectra for gold nanoparticles.

All further data analyses and image reconstruction were performed using MatLab 7.0 (The Mathworks Inc., Natick, MA) and PLS toolbox (Eigenvector Research, Inc.). For principal components analysis (PCA), the first derivatives of the spectra were calculated applying Savitzky−Golay algorithm (number of smoothing points: 5). Vector-normalized first derivatives of the spectra were subjected to PCA, using a spectral range of 300−1700 cm^{-1}. Spectral mapping was based on PCA and *K*-means cluster analysis.[62] As input information for the construction of PCA maps, we used the principal component scores. The number of spectral classes contained in each data set was determined by analyzing the cluster indexes as an output from *K*-means using the MatLab Silhouette plot tool.

For hierarchical cluster analysis, including reconstruction of HCA maps, the cluster algorithm technique of Ward[41] and Euclid-

ean distance $D_{j,k}$ between the ordinate values of spectra X_{ji} and X_{ki} as similarity measure were used. This sum is taken over all selected data points *i*:

$$D_{j,k} = \sqrt{\sum_{i=1}^{n} |X_{ji} - X_{ki}|^2}$$

The algorithm of Ward attempts to find groups merged so that the result will lead to the smallest growth in heterogeneity factor *H,* where $n(i)$ is the number of spectra merged in the object *I* and spectral distance *D:*

$$H(r,i) = D(r,i) = \frac{[n(p) + n(i)]\cdot D(p,i) + [n(i) + n(q)]\cdot D(q,i) - n(i)\cdot D(q,i)}{n + n(i)}$$

Assessment of Cytotoxicity. Cytotoxicity of *p*ABT and 2-NAT was evaluated by utilization of the XTT assay (Biozol Diagnostica, Eching, Germany), where cell viability is spectroscopically determined as the total mitochondrial activity. For this assay, 3T3 cells were seeded in a 96-well culture plate at a density of $\sim 10^4$ cells/well in 200 μL of cell culture medium (DMEM with 10% fetal calf serum) and were incubated for 48 h under controlled conditions (37 °C, 5% CO_2). Then, the culture medium was replaced by fresh medium containing *p*ABT or 2-NAT in a concentration range of 0.1−500 μM. For comparison with the conditions in the Raman experiments, the 3T3 cells were also incubated with the SERS nanoprobes in cell culture medium. Cells not exposed to analyte served as negative controls in each experiment. Positive controls were exposed to 0.01 wt % Triton X-100. After 24 h of incubation, the cells were washed with PBS buffer once and incubated with 100 μL of XTT reagent in DMEM for 4 h. The absorbance of the formed formazan salt was determined using a microplate reader (SpectraMax M5, Molecular Devices, Sunnyvale, U.S.A.) at a wavelength of 460 nm. Cell viability is expressed as ratio of the result obtained with cells exposed to the reporter molecules to those for untreated cells.

Acknowledgment. We thank M. Weller and R. Schneider (BAM Federal Institute for Materials Research and Testing) for use of the cell culture facility and P. Lasch (CytoSpec, Inc.) for providing Cytospec software.

Supporting Information Available: SERS spectra of hybrid probes in cell culture medium. This material is available free of charge *via* the Internet at http://pubs.acs.org.

REFERENCES AND NOTES

1. Campion, A. K., P. Surface-Enhanced Raman Scattering. *Chem. Soc. Rev.* **1998**, *27*, 241–250.
2. Kneipp, K.; Wang, Y.; Kneipp, H.; Itzkan, I.; Dasari, R. R.; Feld, M. S. Population Pumping of Excited Vibrational States by Spontaneous Surface-Enhanced Raman Scattering. *Phys. Rev. Lett.* **1996**, *76*, 2444–2447.
3. Moskovits, M. Surface-Enhanced Spectroscopy. *Rev. Mod. Phys.* **1985**, *57*, 783–826.
4. Otto, A. Surface-Enhanced Raman Scattering: 'Classical' and 'Chemical' Origins. *Light Scattering in Solids IV. Electronic Scattering, Spin Effects, SERS and Morphic Effects*; Cardona, M., Guntherodt, G., Eds.; Springer-Verlag: Berlin, 1984; pp 289−418.
5. Persson, B. N. J. On the Theory of Surface-Enhanced Raman Scattering. *Chem. Phys. Lett.* **1981**, *82*, 561–565.
6. Aroca, R. F.; Alvarez-Puebla, R. A.; Pieczonka, N.; Sanchez-Cortez, S.; Garcia-Ramos, J. V. Surface-Enhanced Raman Scattering on Colloidal Nanostructures. *Adv. Colloid Interface Sci.* **2005**, *116*, 45–61.
7. Cao, Y. W. C.; Jin, R. C.; Mirkin, C. A. Nanoparticles with Raman Spectroscopic Fingerprints for DNA and RNA Detection. *Science* **2002**, *297*, 1536–1540.
8. Jin, R. C.; Cao, Y. C.; Thaxton, C. S.; Mirkin, C. A. Glass-Bead-Based Parallel Detection of DNA Using Composite Raman Labels. *Small* **2006**, *2*, 375–380.
9. Ni, J.; Lipert, R. J.; Dawson, G. B.; Porter, M. D. Immunoassay Readout Method Using Extrinsic Raman Labels Adsorbed on Immunogold Colloids. *Anal. Chem.* **1999**, *71*, 4903–4908.
10. Vo-Dinh, T.; Stokes, D. L.; Griffin, G. D.; Volkan, M.; Kim, U. J.; Simon, M. I. Surface-Enhanced Raman Scattering (SERS) Method and Instrumentation for Genomics and Biomedical Analysis. *J. Raman Spectrosc.* **1999**, *30*, 785–793.
11. Graham, D.; Faulds, K. Quantitative SERRS for DNA Sequence Analysis. *Chem. Soc. Rev.* **2008**, *37*, 1042–1051.
12. Vo-Dinh, T.; Hsin-Neng, W.; Jonathan, S. Plasmonic nanoprobes for SERS biosensing and bioimaging. *J. Biophoton.* **2010**, *3*, 89–102.
13. Schlücker, S.; Küstner, B.; Punge, A.; Bonfig, R.; Marx, A.; Ströbel, P. Immuno-Raman Microspectroscopy: *in Situ* Detection of Antigens in Tissue Specimens by Surface-Enhanced Raman Scattering. *J. Raman Spectrosc.* **2006**, *37*, 719–721.
14. Mulvaney, S. P.; Musick, M. D.; Keating, C. D.; Natan, M. J. Glass-Coated, Analyte-Tagged Nanoparticles: A New Tagging System Based on Detection with Surface-Enhanced Raman Scattering. *Langmuir* **2003**, *19*, 4784–4790.
15. Qian, X. M.; Peng, X. H.; Ansari, D. O.; Yin-Goen, Q.; Chen, G. Z.; Shin, D. M.; Yang, L.; Young, A. N.; Wang, M. D.; Nie, S. M. *in Vivo* Tumor Targeting and Spectroscopic Detection with Surface-Enhanced Raman Nanoparticle Tags. *Nat. Biotechnol.* **2008**, *26*, 83–90.
16. Küstner, B; Gellner, M; Schütz, M; Schöppler, F; Marx, A; Ströbel, P; Adam, P; Schmuck, C; Schlücker, S. SERS Labels for Red Laser Excitation: Silica-Encapsulated SAMs on Tunable Gold/Silver Nanoshells. *Angew. Chem., Int. Ed.* **2009**, *48*, 1950–1953.
17. Kim, J.-H.; Kim, J.-S.; Choi, H.; Lee, S.-M.; Jun, B.-H.; Yu, K.-N.; Kuk, E.; Kim, Y.-K.; Jeong, D.-H.; Cho, M.-H.; Lee, Y.-S. Nanoparticle Probes with Surface Enhanced Raman Spectroscopic Tags for Cellular Cancer Targeting. *Anal. Chem.* **2006**, *78*, 6967–6973.
18. Kneipp, J.; Kneipp, H.; Rajaduraj, A.; Redmond, R. W.; Kneipp, K. Optical Probing and Imaging of Live Cells Using SERS Labels. *J. Raman Spectrosc.* **2009**, *40*, 1–5.
19. Kneipp, J.; Kneipp, H.; Rice, W. L.; Kneipp, K. Optical Probes for Biological Applications Based on Surface Enhanced Raman Scattering from Indocyanine Green on Gold Nanoparticles. *Anal. Chem.* **2005**, *77*, 2381–2385.
20. Gellner, M.; Koempe, K.; Schlücker, S. Multiplexing with SERS Labels Using Mixed SAMs of Raman Reporter Molecules. *Anal. Bioanal. Chem.* **2009**, *394*, 1839–1844.
21. Su, X.; Zhang, J.; Sun, L.; Koo, T. W.; Chan, S.; Sundararajan, N.; Yamakawa, M.; Berlin, A. A. Composite Organic−inorganic Nanoparticles (COINs) with Chemically Encoded Optical Signatures. *Nano Lett.* **2005**, *5*, 49–54.
22. Nithipatikom, K.; McCoy, M. J.; Hawi, S. R.; Nakamoto, K.; Adar, F.; Campbell, W. B. Characterization and Application of Raman Labels for Confocal Raman Microspectroscopic Detection of Cellular Proteins in Single Cells. *Anal. Biochem.* **2003**, *322*, 198–207.
23. Kneipp, J.; Kneipp, H.; Wittig, B.; Kneipp, K. One- and Two-Photon Excited Optical pH Probing for Cells Using Surface-Enhanced Raman and Hyper-Raman Nanosensors. *Nano Lett.* **2007**, *7*, 2819.
24. Stokes, R. J; McKenzie, F; McFarlane, E; Ricketts, A; Tetley, L; Faulds, K; Alexander, J; Graham, D. Rapid Cell Mapping Using Nanoparticles and SERRS. *Analyst* **2009**, *134*, 170–175.
25. Wabuyele, M. B.; Yan, F.; Griffin, G. D.; Vo-Dinh, T. Hyperspectral Surface-Enhanced Raman Imaging of Labeled Silver Nanoparticles in Single Cells. *Rev. Sci. Instrum.* **2005**, 76.
26. Macaskill, A.; Chernonosov, A. A.; Koval, V. V.; Lukyanets, E. A.; Fedorova, O. S.; Smith, W. E.; Faulds, K.; Graham, D. Quantitative Surface-Enhanced Resonance Raman Scattering of Phthalocyanine-Labelled Oligonucleotides. *Nucleic Acids Res.* **2007**, *35*, 1–6.

27. Alvarez-Puebla, R. A.; Dos Santos, D. S.; Aroca, R. F. Surface-Enhanced Raman Scattering for Ultrasensitive Chemical Analysis of 1 and 2-Naphthalenethiols. *Analyst* **2004**, *129*, 1251–1256.
28. Doering, W. E.; Nie, S. M. Spectroscopic Tags Using Dye-Embedded Nanoparticles and Surface-Enhanced Raman Scattering. *Anal. Chem.* **2003**, *75*, 6171–6176.
29. Walt, D. R.; Biran, I. Biosensing with Live Cells Using a High-Density Optical Fiber Array. *Radiat. Res.* **2001**, *156*, 442.
30. Michota, A.; Bukowska, J. Surface-Enhanced Raman Scattering (SERS) of 4-Mercaptobenzoic Acid on Silver and Gold Substrates. *J. Raman Spectrosc.* **2003**, *34*, 21–25.
31. Hildebrandt, P.; Stockburger, M. Surface Enhanced Resonance Raman-Study on Fluorescein Dyes. *J. Raman Spectrosc.* **1986**, *17*, 55–58.
32. Grubisha, D. S.; Lipert, R. J.; Park, H. Y.; Driskell, J.; Porter, M. D. Femtomolar Detection of Prostate-Specific Antigen: An Immunoassay Based on Surface-Enhanced Raman Scattering and Immunogold Labels. *Anal. Chem.* **2003**, *75*, 5936–5943.
33. Wang, Z. Y.; Bonoiu, A.; Samoc, M.; Cui, Y. P.; Prasad, P. N. Biological pH Sensing Based on Surface Enhanced Raman Scattering through a 2-Aminothiophenol-Silver Probe. *Biosens. Bioelectron.* **2008**, *23*, 886–891.
34. Talley, C. E.; Jusinski, L.; Hollars, C. W.; Lane, S. M.; Huser, T. Intracellular pH Sensors Based on Surface-Enhanced Raman Scattering. *Anal. Chem.* **2004**, *76*, 7064–7068.
35. Bereton, R. G. Pattern Recognition. In *Chemometrics: Data Analysis for the Laboratory and Chemical Plant*; John Wiley & Sons Ltd: Chichester, UK, 2006; pp 183−269.
36. Clausen, C.; Wechsler, H. Color Image Compression Using PCA and Backpropagation Learning. *Pattern Recognit.* **2000**, *33*, 1555–1560.
37. Koljenovic, S.; Schut, T. C. B.; van Meerbeeck, J. P.; Maat, A.; Burgers, S. A.; Zondervan, P. E.; Kros, J. M.; Puppels, G. J. Raman Microspectroscopic Mapping Studies of Human Bronchial Tissue. *J. Biomed. Opt.* **2004**, *9*, 1187–1197.
38. Romeo, M. J.; Diem, M. Infrared Spectral Imaging of Lymph Nodes: Strategies for Analysis and Artifact Reduction. *Vib. Spectrosc.* **2005**, *38*, 115–119.
39. Wood, B. R.; Chernenko, T.; Matthaus, C.; Diem, M.; Chong, C.; Bernhard, U.; Jene, C.; Brandli, A. A.; McNaughton, D.; Tobin, M. J.; Trounson, A.; Lacham-Kaplan, O. Shedding New Light on the Molecular Architecture of Oocytes Using a Combination of Synchrotron Fourier Transform-Infrared and Raman Spectroscopic Mapping. *Anal. Chem.* **2008**, *80*, 9065–9072.
40. Pearson, K. On Lines and Planes of Closest Fit to a System of Points in Space. *London, Edinburgh, Philos. Mag. J. Sci.* **1901**, *6*, 559–572.
41. Ward, J. H. Hierarchical Grouping to Optimize an Objective Function. *J. Am. Stat. Assoc.* **1963**, *58*, 236–244.
42. Kneipp, J.; Kneipp, H.; McLaughlin, M.; Brown, D.; Kneipp, K. *in Vivo* Molecular Probing of Cellular Compartments with Gold Nanoparticles and Nanoaggregates. *Nano Lett.* **2006**, *6*, 2225–2231.
43. Bright, N. A.; Reaves, B. J.; Mullock, B. M.; Luzio, J. P. Dense Core Lysosomes Can Fuse with Late Endosomes and Are Re-Formed from the Resultant Hybrid Organelles. *J. Cell Sci.* **1997**, *110*, 2027–2040.
44. Duclos, S.; Corsini, R.; Desjardins, M. Remodeling of Endosomes during Lysosome Biogenesis Involves 'Kiss and Run' Fusion Events Regulated by rab5. *J. Cell Sci.* **2003**, *116*, 907–918.
45. Connor, E. E.; Mwamuka, J.; Gole, A.; Murphy, C. J.; Wyatt, M. D. Gold Nanoparticles Are Taken up by Human Cells but Do Not Cause Acute Cytotoxicity. *Small* **2005**, *1*, 325–327.
46. Khan, J. A.; Pillai, B.; Das, T. K.; Singh, Y.; Maiti, S. Molecular Effects of Uptake of Gold Nanoparticles in HeLa cells. *Chembiochem* **2007**, *8*, 1237–1240.
47. Pan, Y.; Neuss, S.; Leifert, A.; Fischler, M.; Wen, F.; Simon, U.; Schmid, G.; Brandau, W.; Jahnen-Dechent, W. Size-Dependent Cytotoxicity of Gold Nanoparticles. *Small* **2007**, *3*, 1941–1949.
48. Patra, H. K.; Banerjee, S.; Chaudhuri, U.; Lahiri, P.; Dasgupta, A. K. Cell Selective Response to Gold Nanoparticles. *Nanomedicine* **2007**, *3*, 111–119.
49. Pernodet, N.; Fang, X.; Sun, Y.; Bakhtina, A.; Ramakrishnan, A.; Sokolov, J.; Ulman, A.; Rafailovich, M. Adverse Effects of Citrate/Gold Nanoparticles on Human Dermal Fibroblasts. *Small* **2006**, *2*, 766–773.
50. Shukla, R.; Bansal, V.; Chaudhary, M.; Basu, A.; Bhonde, R. R.; Sastry, M. Biocompatibility of gold Nanoparticles and Their Endocytotic Fate Inside the Cellular Compartment: A Microscopic Overview. *Langmuir* **2005**, *21*, 10644–10654.
51. Uboldi, C.; Bonacchi, D.; Lorenzi, G.; Hermanns, M. I.; Pohl, C.; Baldi, G.; Unger, R. E.; Kirkpatrick, C. J. Gold Nanoparticles Induce Cytotoxicity in the Alveolar Type-II Cell Lines A549 and NCIH441. *Part. Fibre Toxicol.* **2009**, *6*, 18.
52. Wang, S. G.; Lu, W. T.; Tovmachenko, O.; Rai, U. S.; Yu, H. T.; Ray, P. C. Challenge in Understanding Size and Shape Dependent Toxicity of Gold Nanomaterials in Human Skin Keratinocytes. *Chem. Phys. Lett.* **2008**, *463*, 145–149.
53. AshaRani, P. V.; Mun, G. L. K.; Hande, M. P.; Valiyaveettil, S. Cytotoxicity and Genotoxicity of Silver Nanoparticles in Human Cells. *ACS Nano* **2009**, *3*, 279–290.
54. Carlson, C.; Hussain, S. M.; Schrand, A. M.; Braydich-Stolle, L. K.; Hess, K. L.; Jones, R. L.; Schlager, J. J. Unique Cellular Interaction of Silver Nanoparticles: Size-Dependent Generation of Reactive Oxygen Species. *J. Phys. Chem. B* **2008**, *112*, 13608–13619.
55. Kawata, K.; Osawa, M.; Okabe, S. *In Vitro* Toxicity of Silver Nanoparticles at Noncytotoxic Doses to HepG2 Human Hepatoma Cells. *Environ. Sci. Technol.* **2009**, *43*, 6046–6051.
56. Yen, H. J.; Hsu, S. H.; Tsai, C. L. Cytotoxicity and Immunological Response of Gold and Silver Nanoparticles of Different Sizes. *Small* **2009**, *5*, 1553–1561.
57. Amrolia, P.; Sullivan, S. G.; Stern, A.; Munday, R. Toxicity of Aromatic Thiols in the Human Red Blood Cell. *J Appl Toxicol* **1989**, *9*, 113–118.
58. Scudiero, D. A.; Shoemaker, R. H.; Paull, K. D.; Monks, A.; Tierney, S.; Nofziger, T. H.; Currens, M. J.; Seniff, D.; Boyd, M. R. Evaluation of a Soluble Tetrazolium Formazan Assay for Cell-Growth and Drug Sensitivity in Culture Using Human and Other Tumor-Cell Lines. *Cancer Res.* **1988**, *48*, 4827–4833.
59. Munro, C. H.; Smith, W. E.; Garner, M.; Clarkson, J.; White, P. C. Characterization of the Surface of a Citrate-Reduced Colloid Optimized for Use as a Substrate for Surface-Enhanced Resonance Raman-Scattering. *Langmuir* **1995**, *11*, 3712–3720.
60. Lee, P. C.; Meisel, D. Adsorption and Surface-Enhanced Raman of Dyes on Silver and Gold Sols. *J. Phys. Chem.* **1982**, *86*, 3391–3395.
61. Lasch, P.; Haensch, W.; Naumann, D.; Diem, M. Imaging of Colorectal Adenocarcinoma Using FT-IR Microspectroscopy and Cluster Analysis. *Biochim. Biophys. Acta* **2004**, *1688*, 176–186.
62. Macqueen, J. B. Some Methods of Classification and Analysis of Multivariate Observations. *Proc. 5th Berkeley Symp. Math. Stat. Prob.* **1967**, *1*, 281–297.